Intrinsic spin-valley locking for conducting electrons in metal-semiconductor-metal lateral heterostructures of 1H-transition-metal dichalcogenides

Tetsuro Habe

Nagamori Institute of Actuators, Kyoto University of Advanced Science, Kyoto 615-8577, Japan

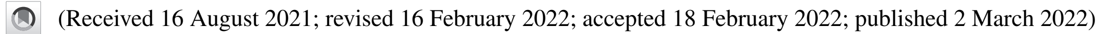
(Received 16 August 2021; revised 16 February 2022; accepted 18 February 2022; published 2 March 2022)

Lateral heterostructures of atomic layered materials alter the electronic properties of pristine crystals and provide a possibility to produce useful monolayer materials. We reveal that metal-semiconductor-metal lateral heterojunctions of 1H-transition-metal dichalcogenides intrinsically possess conducting channels of electrons with spin-valley locking without any extrinsic fabrication breaking the crystal symmetry, e.g., gate electrodes. We theoretically investigate the electronic structure and transport properties of lateral heterojunctions and show that the heterostructure produces conducting channels through the K and K' valleys in the semiconducting transition-metal dichalcogenides and restricts the spin of the conducting electrons in each valley due to the valley-dependent charge transfer effect. Moreover, the theoretical investigation shows that the heterojunction of WSe_2 realizes a high transmission probability for valley-spin locked electrons even in a long semiconducting region. The heterojunction also provides a useful electronic transport property, a steplike I-V characteristic.

DOI: 10.1103/PhysRevB.105.115401

I. INTRODUCTION

Atomic layered materials are solids consisting of atomically thin crystals stacked in layers. Modern experimental techniques enable one to produce atomically thin materials of the layers by cleaving from the bulk crystal, chemical vapor deposition [1,2], chalcogenation [3], or molecular-beam epitaxy [4–6]. These thin layers have attracted much attention because of the fascinating electronic structures different from those of the bulk crystals [7,8]. Moreover, the fabrication techniques to combine different layers into electric or optical systems have been developed in terms of application [9–14]. These atomically thin systems are expected for the realization of atomic layer electric circuits by combining different atomic layered materials.

Transition-metal dichalcogenides (TMDCs) are solids composed of transition-metal and chalcogen atoms and include atomic layered materials in the 1H structure, a crystal structure of monolayer. In 1H-monolayer crystals, electrons possess two degrees of freedom, spin and valley, because of the crystal structure. The manipulation of spin and valley is one of the attractive purposes in the research field of atomic layered materials. Since the spin and valley are coupled due to Zeeman-type spin-orbit coupling in the monolayers, these materials are good candidates for these purposes. The group-VI transition-metal atoms, molybdenum and tungsten, form direct-gap semiconductors in 1H structures with sulfur and selenium [15–17]. On the other hand, 1H crystals of niobium and tantalum, group-V atoms possess metallic properties including an anomalous superconductivity in $NbSe_2$ showing fascinating phenomena [18–22]. In semiconducting 1H-TMDCs, there is spin-valley locking of electrons in the K and K' valleys but the charge injection is necessary to introduce conducting electrons via a gate electrode of field effect transistor (FET), which breaks mirror symmetry of the crystal structure. Although metallic 1H-TMDCs intrinsically possess conducting channels for electrons, there are three valleys and no spin-valley correlation in the Fermi energy. Therefore, neither metallic nor semiconducting TMDCs possess conducting electrons with the spin-valley correlation intrinsically.

In this paper, we theoretically investigate the electronic structure and transport properties of metal-semiconductor-metal lateral heterojunctions of 1H-TMDCs, and show the heterojunctions intrinsically provide the spin-valley locking to conducting electrons as shown in Fig. 1(a). Due to various electronic properties of 1H-TMDCs, heterostructures of these monolayers have been studied for the application to electronic and optical devices in previous experimental papers [11,13,14,23] and theoretical papers [24–26]. The lateral heterostructure is a single layer consisting of different atomic layers as a patchwork, and that of semiconducting 1H-TMDCs has been realized experimentally with atomically aligned interfaces [11,12,27–33]. We consider the lateral heterostructure of metallic and semiconducting TMDCs for providing a fascinating electronic system with spin-valley correlation. For investigating the electronic transport properties, a multiorbital tight-binding model is introduced by referring to the first-principles band structures of the pristine monolayer and periodic stripe lattice of two TMDCs. Moreover, the I-V characteristic of the junction is also theoretically calculated and shows that the heterojunction provides steplike I-V characteristics, a fundamental function in conventional electronics, as shown in Figs. 1(b) and 1(c).

The remaining sections are organized as follows. In Sec. II, the crystal and electronic structures of monolayer NbS_2, $MoSe_2$, and WSe_2 are discussed by using first-principles calculations. The electronic structure of a periodic lateral heterostructure is investigated in Sec. III. Moreover, a

 ©2022 American Physical Society

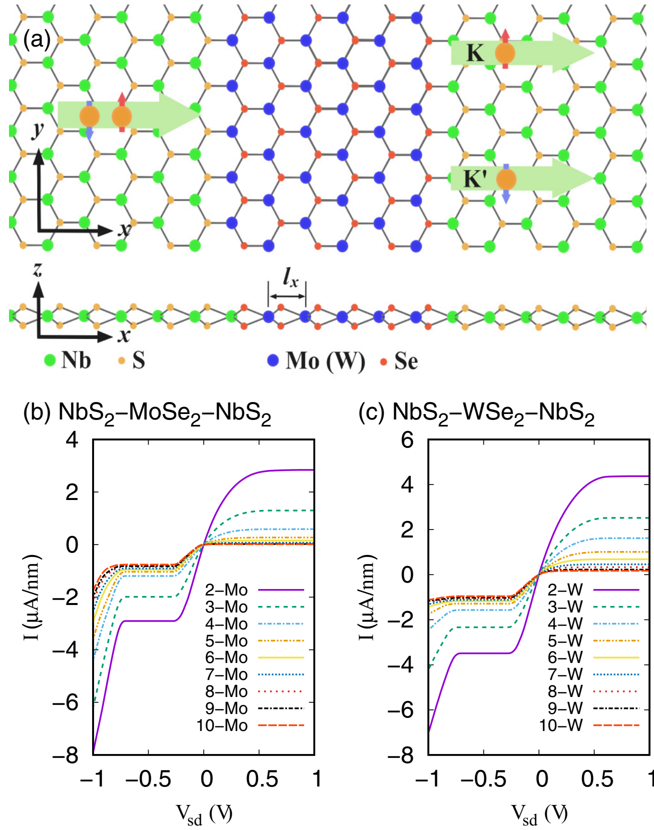

FIG. 1. The schematic of lateral heterojunctions of monolayer TMDCs with two interfaces in (a). The arrows represent the incident spin-unpolarized electronic current and the transmitted electrons with spin-valley locking. In (b) and (c), the I-V characteristics at $T = 10$ K of the heterojunction with 1H-$MoSe_2$ and WSe_2, respectively. The index n in n-Mo and n-W represents the length of semiconducting region nl_x.

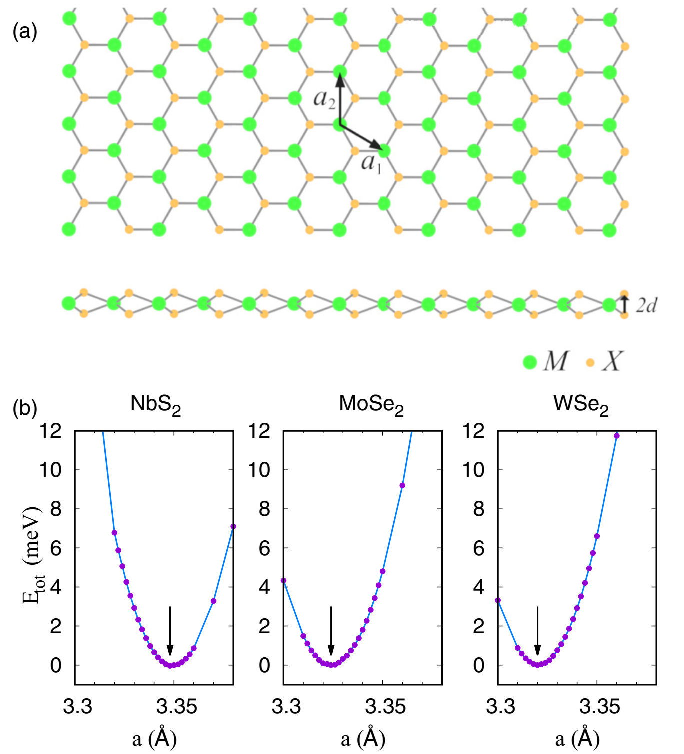

FIG. 2. The schematic of lattice structure of 1H-TMDCs in (a) and the total energy depending on the lattice constants for NbS_2, $MoSe_2$, and WSe_2. The arrow indicates the minimum energy of stable crystal structure in (b). The lattice constant is defined as $a = |\boldsymbol{a}_1| = |\boldsymbol{a}_2|$.

theoretical model is introduced for the study of electronic transport properties. In Sec. IV, the calculation method and numerical results of the electronic transport properties of metal-semiconductor-metal lateral heterojunctions of 1H-TMDCs are provided. In Sec. V, we discuss the relation between the electronic structure and the electronic transport properties and the effect of spin-valley locking on the transport phenomena. The conclusion is given in Sec. VI.

II. CRYSTAL AND ELECTRONIC STRUCTURES OF PRISTINE MONOLAYER CRYSTALS

Monolayer NbS_2, $MoSe_2$, and WSe_2 are classified into 1H crystals and possess a honeycomb lattice structure consisting of three sublayers as shown in Fig. 2(a). In this section, the lattice parameters and electronic structure are presented for these materials by numerical calculations using the first-principles method. Although the electronic structure in a heterojunction varies from that in each pristine crystal, the deviation decreases with increasing distance from the boundary of junction. The calculations are performed by using QUANTUM ESPRESSO, a package of numerical codes for density functional theory (DFT) [34], with the projector augmented-wave method, including spin-orbit coupling within generalized gradient approximation. The energy cutoff is 60 Ry for the plane-wave basis and 400 Ry for the charge density. The convergence criterion 10^{-8} Ry is adopted for the self-consistent field calculation. The lattice parameters of pristine crystals are estimated by comparing the total energy of electronic systems with different lattice parameters. The numerical results for NbS_2, $MoSe_2$, and WSe_2 are presented in Fig. 2. In these calculations, the lattice constant $a = |\boldsymbol{a}_1| = |\boldsymbol{a}_2|$ of a honeycomb structure is considered as a parameter and the distance d between the top and bottom sublayers is simultaneously optimized by the lattice relaxation code in QUANTUM ESPRESSO. The numerical calculations show that the lattice constant a of stable structure is almost the same among the three materials: 3.348 for NbS_2, 3.324 for $MoSe_2$, and 3.320 for WSe_2 within 1%. The numerical results imply the feasibility of commensurate lateral hetero-structures composed of these layered materials with an aligned interface. In Fig. 3, the first-principles band structures of pristine monolayers are presented by applying the optimized lattice parameters for NbS_2, $MoSe_2$, and WSe_2. The first-principles results show the metallic character of NbS_2 and the semiconducting character of $MoSe_2$ and WSe_2. In the semiconducting TMDCs, the top of the valence band splits at the K point due to the Zeeman-type spin-orbit coupling where the heavier transition-metal atom W leads to a larger spin split. The energy dispersion is almost the same among these crystals due to the same crystal structure. In pristine $MoSe_2$ and WSe_2, the Fermi energy is inside the gap and indicates the absence of a conducting

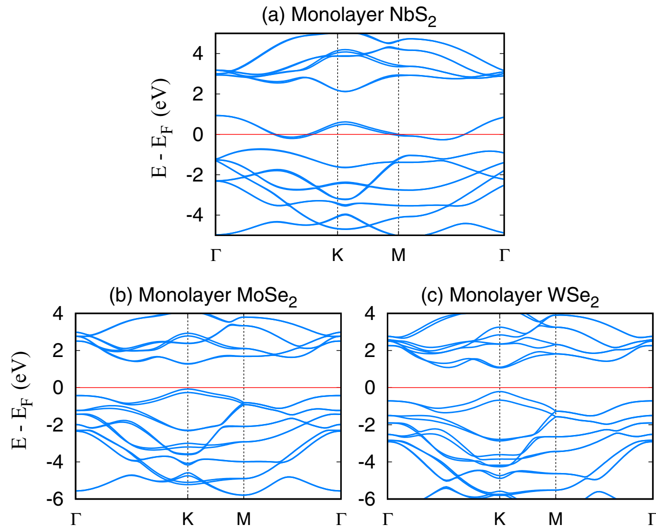

FIG. 3. The electronic band structures of monolayer NbS_2, $MoSe_2$, and WSe_2. The horizontal line indicates the Fermi level.

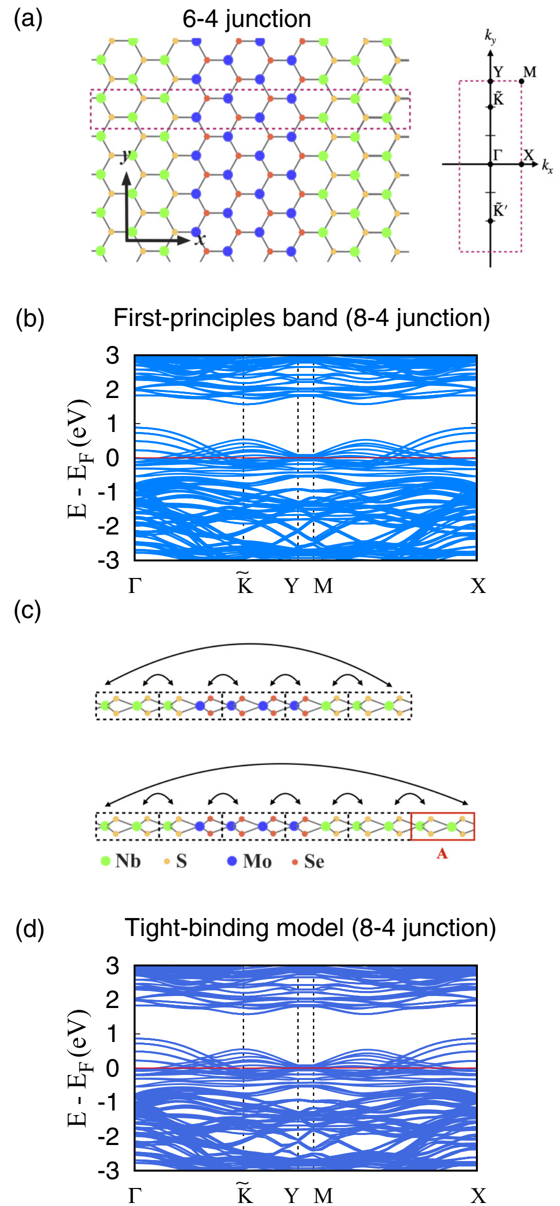

FIG. 4. The schematics and the electronic band structures of a periodic heterostructure of NbS_2 and $MoSe_2$. The unit cell of the periodic structure and the first Brillouin zone are given in (a). Here, $\tilde{K}$ and $\tilde{K}'$ correspond to the K and K' points in the first Brillouin zone of pristine monolayer. In (b), the first-principles band for the heterojunction is given. In (c) and (d), the schematic of tight-binding model and the band structure by using this model are presented.

channel. In the lateral heterojunction, however, the connecting region of these materials can possess conducting channels due to the change of the band structure and the charge transfer through the interface.

III. ELECTRONIC STRUCTURE IN LATERAL HETERO-JUNCTION

In this section, electronic structures in lateral heterojunctions are theoretically analyzed and a theoretical method is introduced for constructing a tight-binding model to investigate electronic transport properties of heterojunctions. The heterojunction consists of two infinitely long metallic monolayer leads and a short semiconducting monolayer sandwiched by the leads as shown in Fig. 1(a). For the investigation, it is necessary to describe electronic states in infinitely long leads where incoming and outgoing electronic waves are traveling. The tight-binding representation enables us to describe these electronic states in such a long system by using finite dimensional hopping matrices. In this paper, the infinitely long junction is divided into three regions: an intermediate scattering region including two boundaries [see Fig. 4(a)] and two half infinite lead regions in a homogeneous crystal structure. In these regions, hopping matrices are obtained by referring to different first-principles bands. The tight-binding model for the whole junction is constructed by connecting these hopping matrices for three regions. The validity of the model is confirmed by comparing the first-principles band and that of the tight-binding model.

A. Electronic structure in periodic junction

The electronic structure of periodic heterojunction of NbS_2 and $MoSe_2$ is investigated. The first-principles bands can be applied to the construction of a tight-binding model in the intermediate region. The unit cell and the first Brillouin zone of a periodic junction are depicted in the left right panels, respectively, of Fig. 4(a). In what follows, these periodic junctions are characterized by the number of transition metal atoms in the unit cell, e.g., the *m*-*n* heterojunction indicates the numbers of Nb and Mo(W) atoms to be *m* and *n*, respectively, in the unit cell. In this paper, the zigzag boundary structure is adopted because the experimentally observed interface is in this structure [11,12,27–33]. In the calculations, the lattice structure is assumed to be commensurate with a unique lattice constant, $a = 3.338$ Å for NbS_2-$MoSe_2$ (3.336 Å for NbS_2-WSe_2), which provides the minimal total energy of electronic system according to the numerical results in Fig. 2.

In Fig. 4(b), the electronic band structure of an 8-4 periodic heterojunction is presented as an example. There is an

energy gap from 1.0 eV to 1.8 eV in the band structure. The subbands below the gap are attributed to the valence band of $MoSe_2$ and the partial filled band of NbS_2. The band structure possesses two local maxima between the Γ and Y points. The local maximum at the Γ point is attributed to that of the Γ valley in the pristine TMDCs and the other local maximum at the $\tilde{K}$ corresponds to the K valley. Thus, the electronic structure implies that the valley degree of freedom is preserved even in the heterojunction. The theoretical model also reveals accumulation of charge transfer between the metallic and semiconducting regions in the K and K' valleys. The local electronic structure in the junction is investigated by using a tight-binding model for the periodic junction where the unit cell is shown in Fig. 4(a). In the tight-binding model, the basis consists of all outer d orbitals in transition-metal atoms and p orbitals in chalcogen atoms within the unit cell. The hopping integrals are calculated by using WANNIER90 [35], a code to compute the maximally localized Wannier orbitals and the hopping matrices between them from a first-principles band structure. For investigating the local structure, the local density of states (LDOS) is evaluated at the atomic position of Mo and Nb atoms for several k_y, where the LDOS is represented by

$$D_{s_z,k_y}(x_j, E_F) = \sum_{n,\alpha,k_x} |\langle\psi_{n,\boldsymbol{k}}|\alpha, s_z, x_j\rangle|^2 \delta(E_F - E_n), \quad (1)$$

with the band index n, the orbital index α in a transition-metal atom at x_j, and the spin index s_z along the z axis. Here, E_n and $|\psi_{n,\boldsymbol{k}}\rangle$ are the eigenenergy and eigenvector, respectively, of the electronic state with $\boldsymbol{k}$ in the nth band. Since electronic states near the Fermi level mainly consist of the d orbitals in transition-metal atoms, the LDOS represents the connectivity of the electronic wave around the junction in the Fermi level.

The numerical results of LDOS in a heterojunction is presented for the up- and down-spin states in Fig. 5, where M, K, and Γ represent k_y corresponding to M, K, and Γ points, respectively, in the pristine crystal. The amplitude in the NbS_2 region is much larger than that in the $MoSe_2$ region. This observation shows that the two regions of $MoSe_2$ and NbS_2 maintain the electronic properties of semiconductor and metal, respectively. In the $MoSe_2$ region, the LDOS is enhanced for up-spin states around the K point. The enhancement is attributed to the charge transfer from the metallic region to the semiconducting region in the K valley, where the valence top appears in the pristine monolayer. Since the electronic structure of the down-spin electron is mirror symmetric in k_y, the down-spin electrons transfer in the K' valley. Therefore, electronic states are connected around the K and K' points with up spin and down spin, respectively, in the Fermi energy through the semiconducting region. The LDOS varies with the atomic species and the length of semiconducting region as shown in Fig. 6. The numerical results show that the LDOS decreases with an increase in the semiconducting region and is enhanced within WSe_2. On the other hand, it remains to be suppressed at the Γ and M points regardless of the length of the semiconducting region. The spatial profile of the LDOS indicates that the heterojunction restricts the electronic transmission to the K and K' valleys. Finally, the stability of the heterostructure is also numerically confirmed by the first-principles calculations. In Fig. 7, the energy difference by forming the junction from the independent flakes of NbS_2 and $MoSe_2$ (WSe_2) is presented for several 6-m heterojunctions. Since, in every 6-m junction, the total energy drops due to formation of the heterostructure, the heterostructure can remain stable. The stability of the heterojunction does not change with the length of the NbS_2 region. The energy difference is enhanced with the length of the semiconducting TMDC and saturates in the 6-10 junction. The saturation indicates that the energy change due to the addition of $MoSe_2$ cells to the long junction is same as that to the pristine $MoSe_2$. This implies that the local electronic structure in the middle area of the $MoSe_2$ region is similar to that of pristine $MoSe_2$.

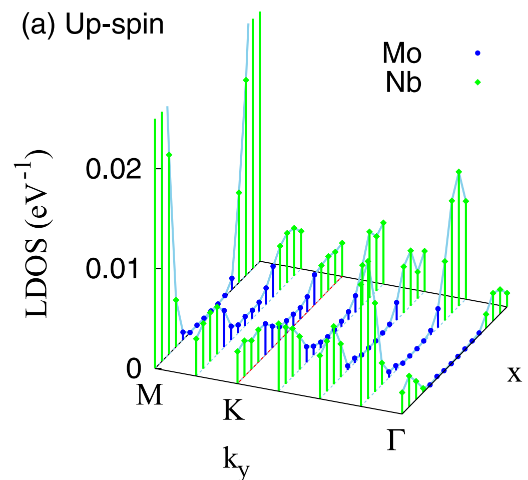

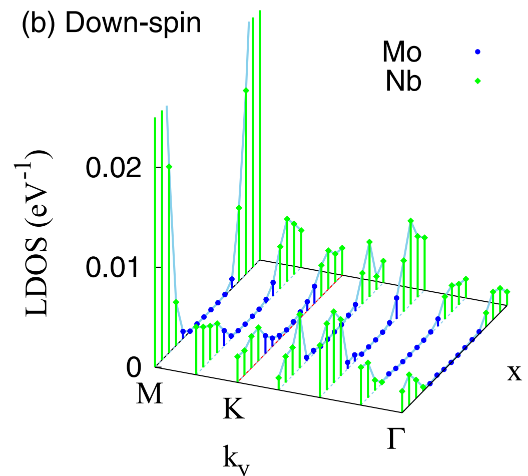

FIG. 5. Spin-resolved LDOS in the Fermi level at the atomic positions of transition metal atoms for heterojunctions of NbS_2 and $MoSe_2$. In the x axis, each point represents the atomic position of the transition metal-atom in the junction direction. In the k_y axis, M, K, and Γ are the k_y components of the wave number corresponding to high-symmetry point for the pristine 1H-crystal.

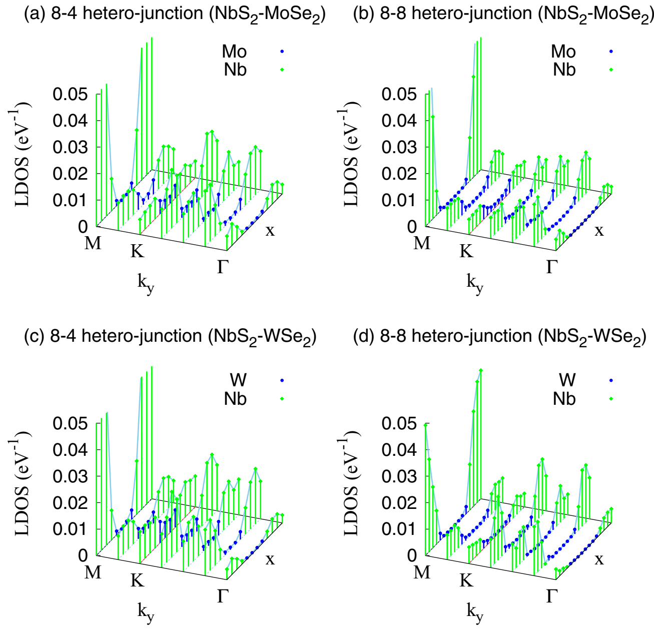

FIG. 6. Total LDOS in 8-n heterojunctions for the Fermi energy. The semiconducting region consists of $MoSe_2$ for (a) and (b) and WSe_2 for (c) and (d).

B. Tight-binding description for heterojunctions

A tight-binding model is constructed for the investigation of electronic transport in heterojunctions by using hopping matrices for the periodic junction and the pristine crystal. A heterojunction is divided into three domains: two leads and an intermediate region including two boundaries. The electronic states in the leads of NbS_2 are described by using the hopping matrices for the pristine crystal.

In the intermediate region, the tight-binding Hamiltonian for the periodic junction is applied to the description. The unit cell contains two transition-metal atoms and four chalcogen atoms as shown in Fig. 4(c) where it is reconstructed by dividing up that of periodic junctions shown in Fig. 4(a). The tight-binding model is represented by

$$H_{k_y}^{(0)} = \sum_{n=1}^{N} \left(c_{k_y,n}^{\dagger}\hat{h}_{k_y,n}^{\dagger}c_{k_y,n} + \left\{c_{k_y,n+1}^{\dagger}\hat{t}_{k_y,n}c_{k_y,n} + \text{H.c.}\right\}\right), \quad (2)$$

where the index n denotes the position of the cell, and $\hat{h}_{k_y,n}$ and $\hat{t}_{k_y,n}$ are the intra- and nearest-neighbor intercell hopping matrices, respectively. The two cells on both sides of the center of the NbS_2 region are adopted as $n = 1$ and $n = N$. Here, $c_{k_y,n}$ is a state vector which consists of the annihilation operators in the spinful Wannier orbitals within the nth cell, where there are ten d orbitals in transition-metal atoms and 12 p orbitals in chalcogen atoms for each spin. In the periodic junction, the periodic boundary condition is given by substituting $c_{k_y,N+1}$ with $c_{k_y,1}$.

The tight-binding Hamiltonian for the infinitely long heterojunction is represented by

$$H_{k_y} = \sum_{n=-\infty}^{\infty} \left(c_{k_y,n}^{\dagger}\hat{h}_{k_y,n}^{\dagger}c_{k_y,n} + \left\{c_{k_y,n+1}^{\dagger}\hat{t}_{k_y,n}c_{k_y,n} + \text{H.c.}\right\}\right), \quad (3)$$

where the hopping matrices for the periodic junction are applied to those in $1 \leqslant n \leqslant N$. The two cells with $n = 1$ and N are connected to the edges of two leads of NbS_2 with the hopping matrix $t_{k_y,-1} = t_{k_y,N} = t_{k_y}$ for the pristine NbS_2. The hopping matrices for the pristine NbS_2 are also applied to those in the cells for $n < 1$ and $N + 1 \leqslant n$. For the smooth connection between the intermediate and lead regions, hopping matrices at the edges of intermediate region should be similar to those in the leads.

By adopting a long NbS_2 region, the local electronic structure in the NbS_2 region of the periodic junction can be similar to that in the pristine crystal. For example, a nearest-neighbor tight-binding model for an 8-4 periodic heterostructure is constructed by using hopping integrals computed from the band structures of a 6-4 periodic heterostructure and pristine monolayer NbS_2. The procedure is schematically depicted in Fig. 4(c). The upper panel represents the schematic of a tight-binding model for the 6-4 periodic heterostructure. To construct the 8-4 model, a hopping matrix from the pristine NbS_2 is introduced in cell A, the middle block in the NbS_2 region, as shown in the lower panel. The intercell hopping from/to cell A is that for the 6-4 periodic heterostructure. In Fig. 4(d), the band structure of the 8-4 heterojunction calculated by using this tight-binding model is presented and is almost same as that from first-principles calculation in Fig. 4(b). The similarity of the two band structures shows that the electronic structure in the NbS_2 region apart from the vicinity of the interface is almost the same as those in the pristine crystal and that the model can well describe electronic states in the 8-4 heterojunction. Therefore, the hopping matrices of the 6-n periodic junction are applied to those in intermediate region of infinitely long heterojunctions.

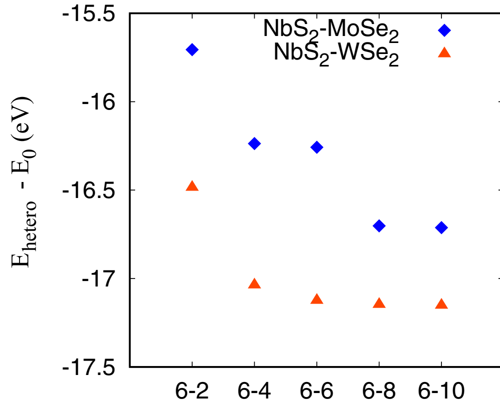

FIG. 7. The energy difference between the junction and the independent flakes of NbS_2 and $MoSe_2$ (WSe_2).

IV. ELECTRONIC TRANSPORT PROPERTY OF METAL-SEMICONDUCTOR-METAL JUNCTION

In this section, the electronic transport properties of a metal-semiconductor-metal lateral hetero junction are theoretically investigated within a two-terminal system. The transmission probability in the heterojunction is calculated by using the lattice Green's function method. The theoretical calculation shows that the heterojunction restricts the spin of transmittable electrons in each valley in the presence of a long semiconducting region. The I-V characteristic is obtained by the Landaurer formula with the transmission probability.

A. Calculation method

The electric current is calculated by the Landauer formula,

$$I=\sum_{m,n}(-e)v_{x,m}[f_F(E_m-E_F)-f_F(E_n-E_F-eV)]T_{nm}, \tag{4}$$

with a source-drain bias V, where $v_{x,m}$ and $f_F(\varepsilon)$ represent the velocity along the x direction and the distribution function, respectively. Here, T_{nm} represents the transmission probability from the incoming state m to the outgoing state n in the left and right half-infinite NbS_2 regions, respectively. Since electrons are scattered in a short intermediate region, the dissipation of electronic energy is ignored, i.e., $E_m=E_n$ in the scattering process. The atomically aligned interface preserves the wave number in the y direction. Therefore, the Landauer formula can be rewritten by using the conductivity $\sigma(\varepsilon)$ for the electronic energy $\varepsilon=E-E_F$,

$$I=\frac{1}{(-e)}\int d\varepsilon[f_F(\varepsilon)-f_F(\varepsilon-eV)]\sigma(\varepsilon), \tag{5}$$

with

$$\sigma(\varepsilon)=\frac{e^2}{h}\int\frac{dk_y}{(2\pi)}\sum_{\mu,\nu}T_{\nu\mu}(\varepsilon,k_y), \tag{6}$$

where the definition of velocity $v_{x,m}=\partial\varepsilon_m/\partial k_x$ is used. Here, the subscripts μ and ν are the indexes to indicate the incoming and outgoing channels in energy ε at wave number k_y.

The transmission probability is computed by using the Green's function method with the multiorbital tight-binding model [10,36,37]. The Green's function describes electronic transfer from an incoming state to an outgoing state in the leads. The wave function $c_{k_y,n}$ in leads is translational symmetric $c_{k_y,n}=\lambda c_{k_y,n-1}$ and represented by

$$\lambda\begin{pmatrix}c_{k_y,n}\\ c_{k_y,n-1}\end{pmatrix}=\begin{pmatrix}t^{-1}_{k_y,0}(h_{k_y,0}-\varepsilon) & -t^{-1}_{k_y,0}t^{\dagger}_{\alpha}\\ 1 & 0\end{pmatrix}\begin{pmatrix}c_{k_y,n}\\ c_{k_y,n-1}\end{pmatrix}, \tag{7}$$

where $h_{k_y,0}$ and $t_{k_y,0}$ are the intra- and intercell hopping matrix in the pristine NbS_2. The wave functions are classified into the right-going states, which have a positive velocity or $|\lambda|<1$, and the left-going states, which have a negative velocity or $|\lambda|>1$. The Green's function for the junction is obtained by using the self-energy in leads,

$$\Sigma_0=\hat{t}_0F_-^{-1},\quad \Sigma_{N+1}=\hat{t}_0^{\dagger}F_+, \tag{8}$$

with

$$F_\pm=U_\pm\Lambda_\pm U_\pm^{-1}, \tag{9}$$

where k_y is omitted from the representation for simplicity. Here, two diagonal matrices $\Lambda_\pm=\mathrm{diag}[\lambda_{1,\pm},\dots,\lambda_{M,\pm}]$ and $U_\pm=[c_{1,\pm},\dots,c_{M,\pm}]$ are introduced, where $\lambda_{j,+(-)}$ and $c_{j,+(-)}$ are the eigenvalue and eigenvector for right (left)-going states, respectively, with the number of Wannier orbitals M in the unit cell. The Green's function $G(\varepsilon)$ for incoming electrons from the left lead is calculated by the following procedure:

$$\begin{aligned}G_{n,0}(\varepsilon)&=G_{n,n}(\varepsilon)\hat{t}_{n-1}G_{n-1,0}(\varepsilon),\\ G_{n,n}(\varepsilon)&=(\varepsilon-\hat{h}_n-\Sigma_n)^{-1},\end{aligned} \tag{10}$$

with $\Sigma_n=\hat{t}_{n-1}G_{n-1,n-1}\hat{t}^{\dagger}_{n-1}$ for $1\leqslant n\leqslant N$ and the connection to the right-lead is given by

$$G(\varepsilon)=(\varepsilon-\hat{h}_0-\Sigma_{N+1}-\hat{t}_NG_{N,N}\hat{t}_N^{\dagger})^{-1}\hat{t}_NG_{N,0}(\varepsilon). \tag{11}$$

The transmission probability is represented by

$$T_{\mu\nu}(\varepsilon)=\sqrt{\frac{v_\mu}{v_\nu}}[U_+^{-1}G(\varepsilon)\hat{t}_0(F_+^{-1}-F_-^{-1})U_+]_{\mu\nu}, \tag{12}$$

where ν and μ are the indexes of incoming and outgoing channels, respectively, and it is calculated for each k_y.

B. Numerical results

First, the wave-number—k_y of the incident electronic wave—dependence of electronic transmission probability is investigated in the Fermi energy. In Fig. 8, the transmission probability is presented for several lengths of the semiconducting region. Here, $T_{\sigma\sigma}(E_F)$ is the mean probability of all incident electrons with spin σ and k_y. Up-spin and down-spin electrons show the inverted profiles in the k_y axis because of the mirror symmetric lattice structure. The numerical results show electrons can transmit through the junction with high probabilities around the K and K' points. Especially in the long semiconducting regions, the electronic transmission in the K (K') valley is permitted for up-spin (down-spin) electrons. In the K' (K) valley, on the other hand, the transmission probability for up-spin (down-spin) electrons rapidly decreases to zero with the length of the semiconducting region. These observations show that the long heterojunction enables us to produce the spin-valley locking for conducting electrons in the metallic TMDC without any exterior equipment, e.g., gate electrode or magnetic substrate, as shown in Fig. 1(a). Moreover, WSe_2 provides a high transmission probability over 0.8 compared with $MoSe_2$ even in the junction with the longest semiconducting region. The heterojunction also provides the spin-valley locking for electrons with various energies through a long semiconducting region. In Fig. 9, the mean transmission probability for up spin is presented for several energies $E<E_F$ in the heterojunction with a long semiconducting region, where the probability for down spin shows the inverted profile in the k_y axis. The numerical calculations for $E>E_F$ are omitted because the electronic transmission is strongly suppressed due to the reduction of the LDOS in the semiconducting region. Large transmission probabilities are observed only around K under all conditions. Especially in the heterojunction of $MoSe_2$, the decrease in

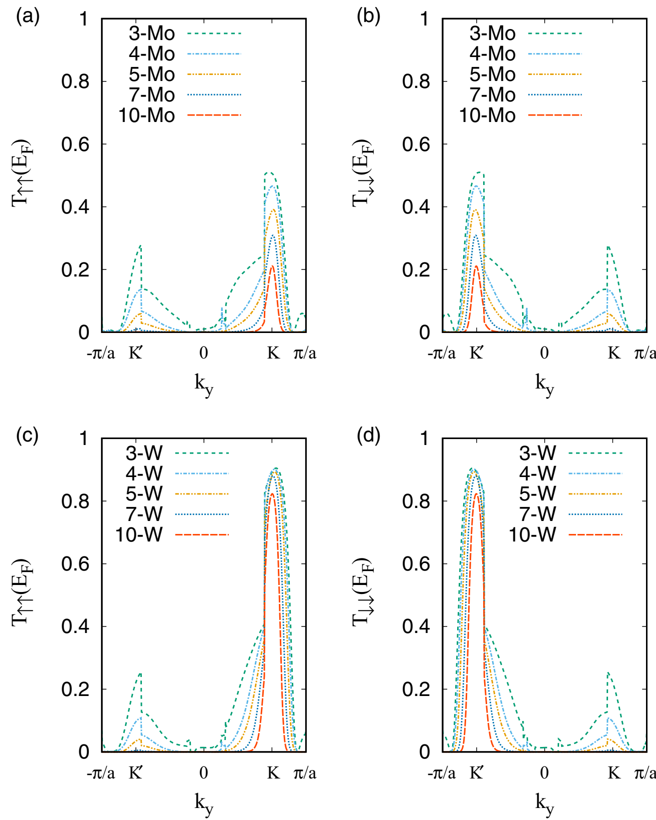

FIG. 8. The electronic transmission probability through the heterojunction of NbS_2-$MoSe_2$-NbS_2 for (a) up spin and (b) down spin, and NbS_2-WSe_2-NbS_2 for (c) up spin and (d) down spin. The curves represent the numerical results for the different lengths of semiconducting region. The left and right panels are the numerical results for up-spin and down spin electrons, respectively.

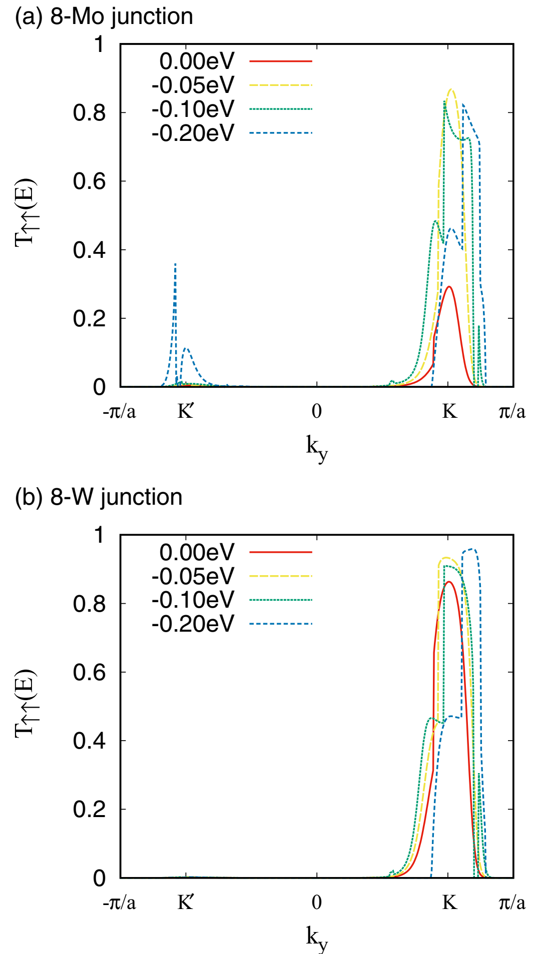

FIG. 9. The mean transmission probability of up-spin electrons with several energies. The energy is defined with respect to the Fermi energy.

E enhances the transmission probability. However, the transmission through $MoSe_2$ is also recovered in the K' valley for $E - E_F < -0.20$ eV, even with the long semiconducting region. These observations indicate the stability of the novel function to provide the spin-valley locking in the heterojunction. The electric conductivity of the heterojunction shows characteristic features corresponding to the electronic structure. The energy dependence of electric conductivity is presented for several heterojunctions of $MoSe_2$ and WSe_2 in Fig. 10, and the I-V characteristic is shown in Fig. 1(b). The conductivity increases with decreasing the length of the semiconducting region in the whole energy region. This observation indicates the increase of transmission probability with shortening $MoSe_2$ or WSe_2 regardless of energy and consistent with the variation of LDOS. In both cases of $MoSe_2$ and WSe_2, there is an insulating energy region independent of the length of intermediate region and the atomic species between -0.7 eV and -0.25 eV. This insulating region corresponds to the flat I-V characteristic in the $V < 0$ and the energy gap between the partially filled band and the lower band of monolayer NbS_2 as shown in Fig. 3(a). Since this energy gap is present in NbS_2 and absent in $NbSe_2$ [38], the insulating energy region, the flat I-V characteristic, is a unique property of NbS_2 leads. The electronic transmission in another insulating energy region in $0 < E - E_F$ is attributed to the electronic properties of the intermediate region of $MoSe_2$ or WSe_2. In the pristine semiconducting TMDCs, there is no conducting channel above the Fermi energy. The small conductivity for $0 < E - E_F$ is attributed to the small LDOS due to the charge transfer from the metallic region.

The I-V characteristics of metal-semiconductor-metal lateral heterojunctions show that the junction possesses an applicable electronic property in classical electronics. In all conditions of the intermediate region, the steplike behavior is observed as a function of the bias voltage and the step height strongly depends on the length of the intermediate region. The electric current, the step height, increases with decreasing the length but the variation is different between the positive and negative voltage regions. In the $V < 0$ region, the nonzero flow remains in junctions with long intermediate lattices of semiconducting TMDCs. The electric current in the $0 < V$ region, on the other hand, decreases to zero with the length. The numerical results show that the rectification effect can be obtained within a monolayer heterojunction by using a long intermediate region. The variation of the I-V characteristic is attributed to the variation of electric conductivity $\sigma(E)$ in the two energy regions.

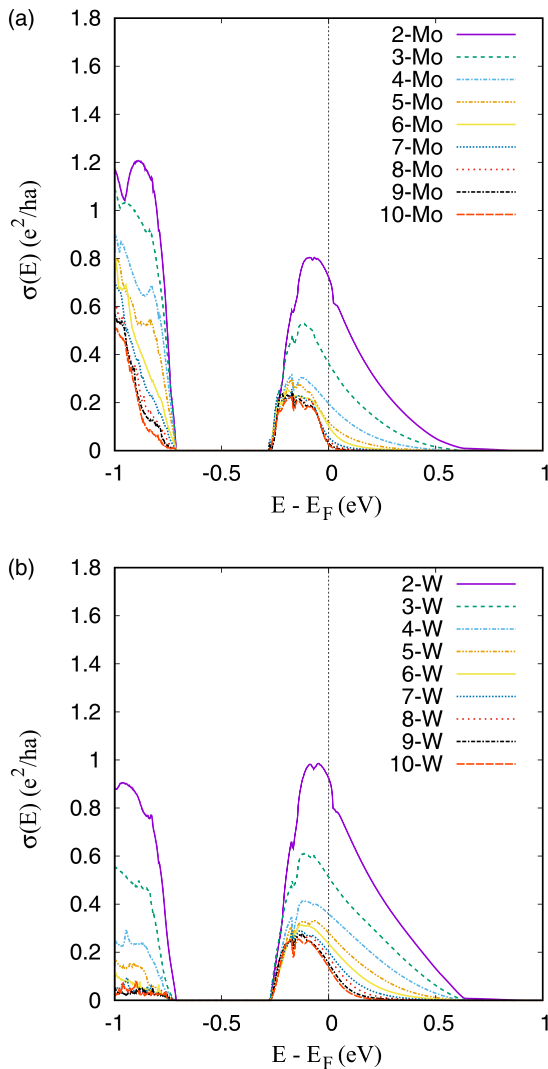

FIG. 10. The electric sheet conductivity of metal-semiconductor-metal lateral heterojunctions. Here, n of n-$MoSe_2$ and n-WSe_2 indicates the length of semiconducting region in units of half the box in Fig. 4(a). In (a) and (b), $MoSe_2$ and WSe_2 are adopted as the material for the semiconducting region.

V. DISCUSSION

In this section, the discussion about the relation between the electronic transport phenomena and the electronic structure is provided. Moreover, a possible effect of spin-valley locking on the electronic transport phenomena is discussed. The numerical calculations show that the NbS_2-$MoSe_2$-NbS_2 and NbS_2-WSe_2-NbS_2 heterojunctions produce the spin-valley locking for conducting electrons. This phenomenon is attributed to the different spin and momentum dependencies of transmission probability. The conducting channels in the NbS_2 region are distributed in three valleys, Γ, K, and K', but they link to another metallic region only in the K and K' valleys through the semiconducting region. The connection of conducting channels can be observed as nonzero LDOS in Fig. 6 and also strongly depends on the electronic spin. This behavior indicates that the charge transfer occurs in the K valley for up-spin electrons and the K' valley for down-spin electrons. In the semiconducting 1H-TMDCs, the highest energy-occupied states appear at the K and K' points in the valence band and they possess the up spin and down spin at the K and K' points, respectively, due to the Zeeman-type spin-orbit coupling. Therefore, electrons in high-energy states transfer to the NbS_2 region and produce the spin-polarized conducting channels around the K and K' points in the semiconducting region.

The spin-valley locking provides the enhancement of electronic transport phenomena related to the Berry curvature. The electronic states in NbS_2 retain a similar structure of Berry curvature to that in semiconducting TMDCs, e.g., MoS_2 [38]. In the K and K' valleys, the Berry curvature increases in intensity and possesses the opposite sign, and it shows the threefold symmetric sign change with a small amplitude in the Γ valley. Since the spin of the transmitted electron is polarized upward in the K valley and downward in the K' valley, the up-spin and down-spin electrons obtain the opposite velocity in the y direction attributed to the Berry curvature. Moreover, conducting electrons in the Γ valley, which are less affected by the Berry curvature, are omitted from electronic transport phenomena. Thus, for example, the heter-junction can provide an intrinsic spin Hall system with a pure spin Hall current, which consists of the opposite flows of up-spin and down-spin electrons. In the pristine metallic 1H-TMDCs, on the other hand, each electronic spin possesses conducting channels in the Γ, K, and K' valleys, and obtains different velocities in the three valleys corresponding to the sign of Berry curvature. Therefore, the semiconducting region of a heterojunction can drastically enhance the spin Hall effect in the metallic TMDC.

VI. CONCLUSION

In this paper, we theoretically investigated the electronic transport properties of metal-semiconductor-metal lateral heterojunctions of 1H-TMDCs and revealed that the semiconducting region enables us to produce spin-valley locking for conducting electrons in the K and K' valleys, and omits electrons in the Γ valley from the electronic transport phenomena. By using first-principles calculations, we show the stability of the heterojunction consisting of NbS_2 and MSe_2 for M=W or Mo. Moreover, the numerical calculations show that the charge transfer occurs between the metallic region and the semiconducting region only in the K and K' valleys, and it produces conducting channels in these valleys. The long semiconducting region permits the nonzero LDOS for up-spin and down-spin electrons in the K and K' valleys, respectively. The electronic transport properties of the heterojunction were investigated by using the lattice Green's function method with a multiorbital tight-binding model obtained from first-principles bands. The theoretical calculations show that the electronic transmission probability strongly depends on the spin and the wave number. Especially in long semiconducting regions, up-spin and down-spin electrons can transmit only in the K and K' valleys, respectively. Therefore, the heterostructure produces a novel electronic system possessing conducting electrons with the intrinsic spin-valley locking. Moreover, it is shown that the heterojunctions are atomically thin materials with a fundamental electronic property, the steplike I-V characteristic, in classical electronics.

[1] Y.-H. Lee, X.-Q. Zhang, W. Zhang, M.-T. Chang, C.-T. Lin, K.-D. Chang, Y.-C. Yu, J. T.-W. Wang, C.-S. Chang, L.-J. Li, and T.-W. Lin, Adv. Mater. **24**, 2320 (2012).
[2] H. Bergeron, V. K. Sangwan, J. J. McMorrow, G. P. Campbell, I. Balla, X. Liu, M. J. Bedzyk, T. J. Marks, and M. C. Hersam, Appl. Phys. Lett. **110**, 053101 (2017).
[3] K.-C. Chen, T.-W. Chu, C.-R. Wu, S.-C. Lee, and S.-Y. Lin, J. Phys. D **50**, 064001 (2017).
[4] E. Moreau, S. Godey, F. J. Ferrer, D. Vignaud, X. Wallart, J. Avila, M. C. Asensio, F. Bournel, and J.-J. Gallet, Appl. Phys. Lett. **97**, 241907 (2010).
[5] L. Zhan, W. Wan, Z. Zhu, T.-M. Shih, and W. Cai, J. Phys.: Conf. Ser. **864**, 012037 (2017).
[6] S. El Kazzi, W. Mortelmans, T. Nuytten, J. Meersschaut, P. Carolan, L. Landeloos, T. Conard, I. Radu, M. Heyns, and C. Merckling, J. Appl. Phys. **123**, 135702 (2018).
[7] A. H. Castro Neto, F. Guinea, N. M. R. Peres, K. S. Novoselov, and A. K. Geim, Rev. Mod. Phys. **81**, 109 (2009).
[8] D. Xiao, G.-B. Liu, W. Feng, X. Xu, and W. Yao, Phys. Rev. Lett. **108**, 196802 (2012).
[9] J. Kang, S. Tongay, J. Zhou, J. Li, and J. Wu, Appl. Phys. Lett. **102**, 012111 (2013).
[10] T. Habe and M. Koshino, Phys. Rev. B **91**, 201407(R) (2015).
[11] M.-Y. Li, Y. Shi, C.-C. Cheng, L.-S. Lu, Y.-C. Lin, H.-L. Tang, M.-L. Tsai, C.-W. Chu, K.-H. Wei, J.-H. He, W.-H. Chang, K. Suenaga, and L.-J. Li, Science **349**, 524 (2015).
[12] M. Najmzadeh, C. Ko, K. Wu, S. Tongay, and J. Wu, Appl. Phys. Express **9**, 055201 (2016).
[13] Y. Son, M.-Y. Li, C.-C. Cheng, K.-H. Wei, P. Liu, Q. H. Wang, L.-J. Li, and M. S. Strano, Nano Lett. **16**, 3571 (2016).
[14] F. Ullah, Y. Sim, C. T. Le, M.-J. Seong, J. I. Jang, S. H. Rhim, B. C. Tran Khac, K.-H. Chung, K. Park, Y. Lee, K. Kim, H. Y. Jeong, and Y. S. Kim, ACS Nano **11**, 8822 (2017).
[15] K. F. Mak, C. Lee, J. Hone, J. Shan, and T. F. Heinz, Phys. Rev. Lett. **105**, 136805 (2010).
[16] W. Jin, P.-C. Yeh, N. Zaki, D. Zhang, J. T. Sadowski, A. Al-Mahboob, A. M. van der Zande, D. A. Chenet, J. I. Dadap, I. P. Herman, P. Sutter, J. Hone, and R. M. Osgood, Phys. Rev. Lett. **111**, 106801 (2013).
[17] Y. Zhang, T.-R. Chang, B. Zhou, Y.-T. Cui, H. Yan, Z. Liu, F. Schmitt, J. Lee, R. Moore, Y. Chen, H. Lin, H.-T. Jeng, S.-K. Mo, Z. Hussain, A. Bansil, and Z.-X. Shen, Nat. Nanotechnol. **9**, 111 (2014).
[18] J. M. Lu, O. Zheliuk, I. Leermakers, N. F. Q. Yuan, U. Zeitler, K. T. Law, and J. T. Ye, Science **350**, 1353 (2015).
[19] X. Xi, Z. Wang, W. Zhao, J.-H. Park, K. T. Law, H. Berger, L. Forro, J. Shan, and K. F. Mak, Nat. Phys. **12**, 139 (2016).
[20] X. Xi, H. Berger, L. Forró, J. Shan, and K. F. Mak, Phys. Rev. Lett. **117**, 106801 (2016).
[21] H. Wang, X. Huang, J. Lin, J. Cui, Y. Chen, C. Zhu, F. Liu, Q. Zeng, J. Zhou, P. Yu, X. Wang, H. He, S. H. Tsang, W. Gao, K. Suenaga, F. Ma, C. Yang, L. Lu, T. Yu, E. H. T. Teo *et al.*, Nat. Commun. **8**, 394 (2017).
[22] T. Habe, Phys. Rev. B **100**, 165431 (2019).
[23] S.-C. Lu, M. Mohamed, and W. Zhu, 2D Mater. **3**, 011010 (2016).
[24] M. Sharma, A. Kumar, P. K. Ahluwalia, and R. Pandey, J. Appl. Phys. **116**, 063711 (2014).
[25] T. Habe, J. Appl. Phys. **126**, 123901 (2019).
[26] T. Deilmann, M. Rohlfing, and U. Wurstbauer, J. Phys.: Condens. Matter **32**, 333002 (2020).
[27] Y. Gong, J. Lin, X. Wang, G. Shi, S. Lei, Z. Lin, X. Zou, G. Ye, R. Vajtai, B. I. Yakobson, H. Terrones, M. Terrones, B. Tay, J. Lou, S. T. Pantelides, Z. Liu, W. Zhou, and P. M. Ajayan, Nat. Mater. **13**, 1135 (2014).
[28] X. Duan, C. Wang, J. C. Shaw, R. Cheng, Y. Chen, H. Li, X. Wu, Y. Tang, Q. Zhang, A. Pan, J. Jiang, R. Yu, Y. Huang, and X. Duan, Nat. Nanotechnol. **9**, 1024 (2014).
[29] C. Huang, S. Wu, A. M. Sanchez, J. J. P. Peters, R. Beanland, J. S. Ross, P. Rivera, W. Yao, D. H. Cobden, and X. Xu, Nat. Mater. **13**, 1096 (2014).
[30] K. Chen, X. Wan, W. Xie, J. Wen, Z. Kang, X. Zeng, H. Chen, and J. Xu, Adv. Mater. **27**, 6431 (2015).
[31] K. Chen, X. Wan, J. Wen, W. Xie, Z. Kang, X. Zeng, H. Chen, and J.-B. Xu, ACS Nano **9**, 9868 (2015).
[32] X.-Q. Zhang, C.-H. Lin, Y.-W. Tseng, K.-H. Huang, and Y.-H. Lee, Nano Lett. **15**, 410 (2015).
[33] Y. He, A. Sobhani, S. Lei, Z. Zhang, Y. Gong, Z. Jin, W. Zhou, Y. Yang, Y. Zhang, X. Wang, B. Yakobson, R. Vajtai, N. J. Halas, B. Li, E. Xie, and P. Ajayan, Adv. Mater. **28**, 5126 (2016).
[34] P. Giannozzi, S. Baroni, N. Bonini, M. Calandra, R. Car, C. Cavazzoni, D. Ceresoli, G. L. Chiarotti, M. Cococcioni, I. Dabo, A. Dal Corso, S. de Gironcoli, S. Fabris, G. Fratesi, R. Gebauer, U. Gerstmann, C. Gougoussis, A. Kokalj, M. Lazzeri, L. Martin-Samos *et al.*, J. Phys.: Condens. Matter **21**, 395502 (2009).
[35] A. A. Mostofi, J. R. Yates, Y.-S. Lee, I. Souza, D. Vanderbilt, and N. Marzari, Comput. Phys. Commun. **178**, 685 (2008).
[36] T. Ando, Phys. Rev. B **44**, 8017 (1991).
[37] T. Habe and M. Koshino, Phys. Rev. B **93**, 075415 (2016).
[38] T. Habe, Phys. Rev. B **102**, 195430 (2020).